

Precision calculations of the gravitational wave background spectrum from inflation

Sachiko Kuroyanagi,^{1,*} Takeshi Chiba,² and Naoshi Sugiyama^{1,3}

¹*Department of Physics, Nagoya University, Chikusa, Nagoya 464-8602, Japan*

²*Department of Physics, College of Humanities and Sciences, Nihon University, Tokyo 156-8550, Japan*

³*Institute for Physics and Mathematics of the Universe, University of Tokyo,
5-1-5 Kashiwa-no-ha, Kashiwa City, Chiba 277-8582, Japan*

The spectrum of the gravitational wave background originating from quantum fluctuations during inflation is calculated numerically for various inflation models over a wide range of frequencies. We take into account four ingredients : the scalar field dynamics during inflation making no use of the slow-roll approximation, the fermionic decay of the scalar field with a small coupling constant during the reheating process, the change of the effective number of degrees of freedom g_* in the radiation-dominated era, and the anisotropic stress of free-streaming neutrinos. By numerically solving the evolution of gravitational waves during and after inflation up to the present, all of these effects can be examined comprehensively and accurately over a broad spectrum, even at very high frequencies. We find that the spectrum shows (i) a large deviation from the spectrum less accurate obtained by Taylor expanding around the CMB scale using the slow-roll approximation (ii) a characteristic frequency dependence due to the reheating effect, and (iii) damping due to the g_* changes and the neutrino anisotropic stress. We suggest that future analysis of the gravitational-wave background should take into consideration the fact that analytical estimates using the Taylor expansion overestimate the amplitude of the spectrum.

PACS numbers: 98.80.Cq, 04.30.-w

I. INTRODUCTION

Inflation [1, 2, 3] is now widely considered to be the most attractive scenario for describing the early evolution of the universe. One of the reasons why inflation succeeds as a standard paradigm is that it not only solves conundrums in the big bang theory (horizon/flatness/monopole problems) but also predicts an almost scale-invariant spectrum of scalar (density) perturbations originating from quantum fluctuations [4, 5, 6]. This theoretical prediction is consistent with large-scale structure and cosmic microwave background (CMB) observations, and there have been intensive attempts to obtain a deeper understanding of inflation dynamics through analysis of these observations. Moreover, inflation also generates an almost scale-invariant spectrum of tensor perturbations (gravitational waves) [7, 8, 9], the detection of which is expected to provide a new source of information on the early universe, and provide a key to discriminate between inflation and alternative models. There are ongoing efforts to detect indirectly this inflation-produced gravitational wave background, such as the next-generation CMB experiments which measure CMB polarization patterns induced by gravitational waves [10, 11]. Clearly, the direct detection [12, 13, 14, 15, 16, 17] of the primordial gravitational wave background would provide an even more attractive prospect.

The most striking property of gravitational waves is their weakness of interaction with matter. While this property makes direct detection very difficult, it may

provide the following specific benefits. Since primordial gravitational waves propagate freely since the end of inflation because of their weak interactions with matter, one may observe a remnant of inflation directly through observation. In addition, due to the smallness of their amplitude, a linear approximation is valid for gravitational waves in all scales. This makes it easy to study their behaviour at any frequency. This is in contrast to density perturbations, whose evolution is more complicated, and which have now grown non-linear at small scales. (Although gravitational waves are affected by the second order term of the primordial density perturbations [18] and the growing non-linear modes [19] through the anisotropic stress term, these effects appear at very low frequencies ¹ ($\lesssim 10^{-15}\text{Hz}$) and have been estimated to be small.) Therefore, the gravitational wave background has the potential to allow us to extract "clean" information from the early universe, and is extremely attractive as a tool of future observational cosmology.

In this paper, our goal is to provide precise predictions for the spectrum amplitude of the gravitational wave background as preparation for assessing detectability in future experiments aiming at the direct detection of gravitational waves. It is a well-known fact that the tilt and the amplitude of the spectrum strongly depend on the in-

¹ One might expect more gravitational waves are generated on smaller scales due to the non-linear structure formation since the structure becomes nonlinear from the smaller scales in the CDM model. However, it is not the case because the amplitude of the gravitational waves generated at high redshift decreases while they propagate in the expanding universe, and becomes negligible small. (See Ref. [19], for details.)

*s-kuro@a.phys.nagoya-u.ac.jp

flation model. Also, after inflation, changes in the Hubble expansion rate and the anisotropic stress of neutrinos induce characteristic features in the spectrum [20, 21]. These components which affect the spectrum should be considered all together to estimate accurately the amplitude of the spectrum over a wide frequency range. The latter effects have been well investigated at frequencies below 10^{-2}Hz by Watanabe and Komatsu [22], who calculate the spectrum taking into account both the change of the effective number of degrees of freedom and the neutrino anisotropic stress. In contrast, our interest lies particularly in the higher-frequency region of the gravitational wave background spectrum.

The reason why we focus on the high frequency modes is that they are sensitive to a crucial aspect of the dynamics of inflation: how inflation terminates. The high frequency modes are produced outside the horizon near the end of inflation and re-enter the horizon soonest after inflation ends, in the period where reheating is considered to occur. Since the amplitude of a gravitational-wave mode is affected by the Hubble expansion rate at the point when that mode crosses the horizon, the spectrum of these modes depends on the particular inflation and reheating models chosen. This means that it may be possible to extract information about the epoch, which is still quite unclear, through direct detection of the gravitational wave background.

In this paper, we numerically analyze the spectrum of the primordial gravitational wave background for several inflation models. It is particularly worth noting that the dynamics of inflation and reheating are included by numerically solving the relevant equations, which describe an inflaton field rolling down its potential and subsequently decaying into radiation with oscillation at the bottom of the potential. This means that we make no use of the slow-roll approximation, which is no longer valid near the end of inflation, unlike many previous works [23, 24, 25, 26]. Our numerical approach for computing the dynamics of inflation enables us to find the deviation from this approximation, which depends strongly on the inflation model. Moreover this numerical approach works effectively to connect the change of the Hubble expansion rate smoothly from the inflation phase to the radiation dominated era via the reheating process, which cannot be accurately treated analytically. Since the Hubble expansion rate depends on the behavior of the scalar field and following reheating process, the amplitude of the high frequency modes are determined by a combination of both the dynamics of inflation and the reheating mechanism. Detailed numerical calculations of these processes are therefore required in order to examine precisely the high frequency gravitational waves which are the main subject of this paper.

In our calculation, we take into account the change of the effective number of degrees of freedom and the neutrino anisotropic stress, both of which cause a damping of the spectrum. It is notable that our detailed calculations have also revealed a numerical error due to the

inaccurate treatment of the effect of neutrino anisotropic stress in previous work (Ref. [22]). As a result, we obtain a wide range spectrum which shows interesting features produced in the early universe; the inflationary phase and the reheating phase. We should therefore stress that this is the first work which calculates the amplitude of the gravitational wave background accurately including all of the factors that are definitely understood to affect it. This makes it possible to obtain an accurate spectral amplitude and is therefore essential for accurately assessing the detectability of the gravitational wave background.

The outline of our paper is as follows. In Sec.II, we begin with the evolution equations expressing gravitational waves in terms of metric tensor perturbations. Then we review the basics of the gravitational wave background spectrum and evaluate the basic spectrum shape analytically. In Sec.III, we describe the physical phenomena in the early universe that are thought to have affected the spectrum shape. In Sec.IV, we present the results of our numerical calculations of the gravitational wave background spectrum and provide comparisons with theoretical predictions. We also show the results at different reheating temperatures and different inflation models. In Sec.V, we conclude with a discussion of the results of Sec.IV.

II. THE EVOLUTION OF GRAVITATIONAL WAVES IN THE EXPANDING UNIVERSE

Gravitational waves in the expanding universe can be described as a transverse-traceless part of the metric perturbation in a Friedmann Robertson-Walker background. We consider the spatially flat case in which the line element is given by

$$ds^2 = -dt^2 + a^2(t)(\delta_{ij} + h_{ij})dx^i dx^j, \quad (1)$$

where the tensor perturbations h_{ij} satisfy the transverse-traceless conditions, $h_{00} = h_{0i} = \partial^i h_{ij} = h^i_i = 0$. Applying the metric of this space-time to the perturbed Einstein equation $\delta G_{ij} = 8\pi G\delta T_{ij}$, we obtain the equation of motion for gravitational waves

$$\ddot{h}_{ij} + 3H\dot{h}_{ij} - \frac{1}{a^2}\nabla^2 h_{ij} = 16\pi G\Pi_{ij}, \quad (2)$$

where the over-dot describes the time derivative, H is the Hubble parameter, and Π_{ij} is the transverse-traceless part of the anisotropic stress of the energy-momentum tensor. The obvious contribution from the anisotropic stress term is the damping effect due to neutrino free-streaming, presented in Ref. [21, 22, 23, 27]. We take into account this effect numerically solving the integro-differential equation shown in Appendix C. Although there may be other yet unknown free-streaming particles which cause damping at higher frequencies, we do not include such an uncertain component.

We now develop the basics of the gravitational wave background spectrum assuming a perfect fluid $\Pi_{ij} = 0$

for simplicity. For convenience, we decompose h_{ij} into its Fourier modes with the comoving wave number \mathbf{k} and denote the two independent polarization states as

$$h_{ij}(t, \mathbf{x}) = \sum_{\lambda=+, \times} \int \frac{d^3k}{(2\pi)^{3/2}} \epsilon_{ij}^\lambda(\mathbf{k}) h_{\mathbf{k}}^\lambda(t, \mathbf{k}) e^{i\mathbf{k} \cdot \mathbf{x}}. \quad (3)$$

where the polarization tensors $\epsilon_{ij}^{+, \times}$ satisfies symmetric and transverse-traceless condition and are normalized as $\sum_{i,j} \epsilon_{ij}^\lambda (\epsilon_{ij}^{\lambda'})^* = 2\delta^{\lambda\lambda'}$. Then Eq. (2) becomes

$$\ddot{h}_{\mathbf{k}}^\lambda + 3H\dot{h}_{\mathbf{k}}^\lambda + \frac{k^2}{a^2} h_{\mathbf{k}}^\lambda = 0. \quad (4)$$

Note that, by neglecting the anisotropic stress term, the contribution of other components in the universe appears only through the second term. This means we can follow the evolution of gravitational waves with Eq.(4) simply by computing the Hubble expansion rate, the evolution of which is determined by the total energy densities of the background components.

Let us briefly explain how the primordial gravitational waves evolve in the expanding universe. Initially, during inflation, the modes of interest were deep inside the Hubble horizon ($k \gg aH$) and fluctuating quantum-mechanically. During this phase, the amplitude of $h_{\mathbf{k}}^\lambda$ is determined according to Appendix A,

$$|h_{\mathbf{k}}^\lambda|^2 = \frac{16\pi G}{2ka^2}. \quad (5)$$

As the universe expands exponentially, the mode crosses outside the horizon ($k < aH$). At this moment, we assume that the quantum fluctuations become classical. Using the fact that the second term in Eq. (4) becomes dominant compared with the third term, one can easily obtain the solution

$$h_{\mathbf{k}}^\lambda \propto \text{const.} \quad (6)$$

After the end of inflation, the mode re-enters the horizon ($k > aH$) and starts to oscillate. In this phase, the behavior of $h_{\mathbf{k}}^\lambda$ is described by the WKB solution (see Appendix B),

$$h_{\mathbf{k}}^\lambda \propto a^{-1} e^{\pm i k \tau}, \quad (7)$$

where τ is the conformal time defined by $d\tau \equiv a(t)dt$.

We now define a dimensionless quantity to characterize the strength of gravitational waves in terms of their energy density ρ_{GW} and the critical density of the universe $\rho_c \equiv 3H^2/8\pi G$ [28],

$$\begin{aligned} \Omega_{\text{GW}} &\equiv \frac{1}{\rho_c} \frac{d\rho_{\text{GW}}}{d \ln k} \\ &= \frac{1}{12} \left(\frac{k}{aH} \right)^2 \frac{k^3}{\pi^2} \sum_{\lambda} |h_{\mathbf{k}}^\lambda|^2. \end{aligned} \quad (8)$$

In the second step, we have substituted the Fourier transformed form of ρ_{GW} , which is given by the 00-component

of the stress-energy tensor as follows,

$$\begin{aligned} \rho_{\text{GW}} &= \frac{1}{64\pi G a^2} \langle (\partial_\tau h_{ij})^2 + (\vec{\nabla} h_{ij})^2 \rangle \\ &= \frac{1}{32\pi G} \int \frac{d^3k}{(2\pi)^3} \frac{k^2}{a^2} 2 \sum_{\lambda} |h_{\mathbf{k}}^\lambda|^2. \end{aligned} \quad (9)$$

Here, we have assumed that the mode is inside the horizon and behaves like Eq. (7), which means that the conformal-time derivative of the mode can be regarded as the same as the spatial derivative when taking the spatial average, $\langle \dots \rangle$.

One may define the tensor power spectrum $\mathcal{P}_T(k)$ in terms of the primordial tensor power spectrum $\mathcal{P}_{T,\text{prim}}(k)$ and the tensor transfer function $T_T(k)$ as

$$\mathcal{P}_T(k) \equiv \frac{k^3}{\pi^2} \sum_{\lambda} |h_{\mathbf{k}}^\lambda|^2 = \mathcal{P}_{T,\text{prim}}(k) T_T^2(k). \quad (10)$$

Then the energy spectrum Ω_{GW} can be rewritten as

$$\Omega_{\text{GW}} = \frac{1}{12} \left(\frac{k}{aH} \right)^2 \mathcal{P}_{T,\text{prim}}(k) T_T^2(k). \quad (11)$$

This expression is used in previous works because it is useful to evaluate the spectrum by splitting the contributions to the spectrum shapes into two parts, $\mathcal{P}_{T,\text{prim}}(k)$ and $T_T(k)$. The spectrum shape is affected by the Hubble rate both when the mode leaves the horizon during inflation and when the mode re-enters the horizon after inflation. Since $\mathcal{P}_{T,\text{prim}}(k)$ is the spectrum at the end of inflation, it contains only the contribution from the former, whereas $T_T(k)$ represents the time evolution of each mode after the end of inflation, which means it contains only the contribution from latter. In most previous work, $\mathcal{P}_{T,\text{prim}}(k)$ has been evaluated analytically using the slow-roll approximation. We shall return to this in the next section.

We now show two simple examples of frequency dependence of the spectrum – a radiation-dominated and a matter-dominated cases – assuming the primordial spectrum is flat, $\mathcal{P}_{T,\text{prim}}(k) \propto k^0$. According to Eq. (6), $h_{\mathbf{k}}^\lambda$ remains constant on super-horizon scales. This means the transfer function can be written in terms of the amplitude of $h_{\mathbf{k}}^\lambda$ at horizon crossing, $T_T^2(k) = |h_{\mathbf{k},0}|^2 / |h_{\mathbf{k},\text{hc}}|$, where the subscript "0" denotes the present time and "hc" denotes the horizon-crossing time. After the modes re-enter the horizon, $h_{\mathbf{k}}^\lambda$ decreases inversely proportional to the scale factor, so that $|h_{\mathbf{k},0}| = |h_{\mathbf{k},\text{hc}}| (a_{\text{hc}}/a_0)$, then we get $T_T^2(k) = a_{\text{hc}}^2/a_0^2$. Therefore, the energy spectrum at the present time is rewritten as $\Omega_{\text{GW},0} = (k^2/12a_0^2 H_0^2) \mathcal{P}_{T,\text{prim}}(a_{\text{hc}}^2/a_0^2)$. By using the relation $k = a_{\text{hc}} H_{\text{hc}}$, the value a_{hc} in $\Omega_{\text{GW},0}$ can be converted into k with the proportional relation between a_{hc} and H_{hc} . During a radiation-dominated era, the Hubble rate behaves as $H \propto a^{-2}$. This leads to $a_{\text{hc}} \propto k^{-1}$, then we obtain

$$\Omega_{\text{GW},0} \propto k^0. \quad (12)$$

Similarly, during a matter-dominated era, $H \propto a^{-3/2}$ leads to $a_{\text{hc}} \propto k^{-2}$, then we obtain

$$\Omega_{\text{GW},0} \propto k^{-2}. \quad (13)$$

III. PHYSICS OF THE EARLY UNIVERSE AND ITS EFFECT ON THE SPECTRUM

As was seen in the previous section, the evolution of the Hubble expansion rate is important to determine the shape of the gravitational wave background spectrum. Here, we shall describe the physics of the early universe which affect the spectrum shape and provide the equations necessary for calculating the evolution of the Hubble rate.

A. Slow-roll inflation

In most models of inflation, the accelerated expansion is driven by a scalar field ϕ whose equation of motion is given by

$$\ddot{\phi} + 3H\dot{\phi} + V' = 0, \quad (14)$$

where prime denotes derivative with respect to ϕ . The Hubble parameter is determined by the energy density of this scalar field, $\rho_\phi = \dot{\phi}^2/2 + V$, so that the Friedmann equation can be written as

$$H^2 = \frac{8\pi}{3m_{Pl}^2} \left(\frac{1}{2}\dot{\phi}^2 + V(\phi) \right), \quad (15)$$

where $m_{Pl} = \sqrt{G}$ is the Planck mass. For exponential expansion, the energy density of the ϕ field should be dominated by its potential energy, $\dot{\phi}^2/2 \ll V$. This condition is often characterized by the slow-roll parameters which are defined as

$$\epsilon \equiv \frac{m_{Pl}^2}{16\pi} \left(\frac{V'}{V} \right)^2, \quad (16)$$

$$\eta \equiv \frac{m_{Pl}^2}{8\pi} \frac{V''}{V}. \quad (17)$$

As long as the so-called slow-roll conditions, $\epsilon \ll 1$ and $|\eta| \ll 1$, are satisfied, inflation continues keeping the Hubble rate nearly constant and we can use the slow-roll approximation which is a useful tool to theoretically study the fluctuations generated during inflation.

In the slow-roll regime, the spectra of the primordial scalar perturbation $\mathcal{P}_{S,\text{prim}}(k)$ and tensor perturbation $\mathcal{P}_{T,\text{prim}}(k)$ which are generated outside the horizon can be derived as

$$\mathcal{P}_{S,\text{prim}}(k) = \frac{1}{\pi\epsilon} \left(\frac{H}{m_{Pl}} \right)^2 \bigg|_{k=aH}, \quad (18)$$

$$\mathcal{P}_{T,\text{prim}}(k) = \frac{16}{\pi} \left(\frac{H}{m_{Pl}} \right)^2 \bigg|_{k=aH}, \quad (19)$$

where H is evaluated at the time when the mode with wave number k exits the horizon. To parametrize the deviation from scale invariance of the tensor spectrum $\mathcal{P}_{T,\text{prim}}(k)$, one may use the tensor spectral index n_T and its running α_T which can be expressed in terms of the slow-roll parameters [29, 30],

$$n_T(k) \equiv \frac{d \ln \mathcal{P}_{T,\text{prim}}(k)}{d \ln k} \simeq -2\epsilon, \quad (20)$$

$$\alpha_T(k) \equiv \frac{dn_T}{d \ln k} \simeq 4\epsilon\eta - 8\epsilon^2. \quad (21)$$

Then the power spectrum is represented in an expanded form in terms of $\ln(k/k_0)$,

$$\ln \frac{\mathcal{P}_{T,\text{prim}}(k)}{\mathcal{P}_{T,\text{prim}}(k_0)} = n_T(k_0) \ln \frac{k}{k_0} + \frac{1}{2} \alpha_T(k_0) \ln^2 \frac{k}{k_0} + \dots, \quad (22)$$

where k_0 is a pivot wavenumber. Also, the tensor-to-scalar ratio can be written in terms of ϵ ,

$$r \equiv \frac{\mathcal{P}_{T,\text{prim}}(k)}{\mathcal{P}_{S,\text{prim}}(k)} \simeq 16\epsilon. \quad (23)$$

These expressions are used as a reference for comparison with our numerical results in the subsequent section.

B. Reheating process

During reheating process that follows inflation, the energy of the scalar field is transferred to radiation or other light particles oscillating near the minimum of its potential. Here, we consider the perturbative decay of the scalar field [31, 32] and only consider the interaction between the scalar field and light fermions. Then the equations for ϕ can be simply rewritten including the decay term as [33, 34]

$$\ddot{\phi} + (3H + \Gamma)\dot{\phi} + V' = 0, \quad (24)$$

where Γ is the decay rate of ϕ particle, which depends on oscillation frequency at the bottom of the potential. Note that this expression is valid only for the case where the mass of the interacting field and the decay rate Γ is sufficiently smaller than the oscillation frequency of the ϕ field. We do not deal with non-linear processes like preheating [35, 36], which occurs if the decay is bosonic and the parameters satisfy specific conditions [34]. Such processes may also generate gravitational waves at high frequencies with a quite different spectrum shape, and may even exceed the amplitude of the inflation-produced gravitational wave background [37, 38, 39]. However, since we aim to provide a conservative estimate of the spectrum, we only consider perturbative process which exist regardless of the chosen reheating scenario.

The additional set of equations to describe the reheating process is as follows. The evolution equation for the radiation energy density ρ_r can be written as

$$\dot{\rho}_r + 4H\rho_r = \Gamma\rho_\phi. \quad (25)$$

The Friedmann equation is written in terms of the energy density of the ϕ field and radiation field,

$$H^2 = \frac{8\pi}{3m_{Pl}^2}(\rho_\phi + \rho_r). \quad (26)$$

Therefore, using this sets of three equations, Eqs. (24),(25) and (26), we can simply calculate the Hubble rate following the evolution of both the scalar field and the radiation field which are interacting with each other.

Reheating ends around $\Gamma \sim H$ where the ϕ field begins to decay exponentially. At this stage, the universe becomes well radiation-dominated, so that we can define the reheating temperature which can be related to Γ [33],

$$T_{RH} \sim g_*^{-\frac{1}{4}} \left(\frac{45}{8\pi^3} \right)^{\frac{1}{4}} (m_{Pl}\Gamma)^{\frac{1}{2}}, \quad (27)$$

where $g_*(T)$ is the effective number of degrees of freedom. This value is often used to characterize the reheating process.

C. Thermodynamics of the radiation era

After the universe becomes radiation-dominated, the Hubble rate basically behaves as $H \propto a^{-2}$. In the early stages of the radiation-dominated era, particles in the universe are relativistic and contribute to the radiation energy density. However, when a particle species becomes non-relativistic as the universe expands and the temperature decreases, the contribution of the particle species to the radiation drops exponentially and becomes negligible. This results in the change of the radiation energy density and the evolution of the Hubble rate, then induces a damping of the amplitude at high frequencies. These processes for all particle species are treated in the framework of thermodynamics as changes of the "effective number of relativistic degrees of freedom", $g_*(T)$, which is introduced for the convenience to evaluate the contribution of all relativistic species as a whole. We take into account this effect with a formulation based on Ref. [33] which is briefly described as follows.

During the radiation era, matter particles are in thermal equilibrium and they obey Fermi-Dirac or Bose-Einstein statistics. In this case, the energy density and the entropy density at temperature T can be expressed as

$$\rho(T) = \frac{\pi^2}{30} g_*(T) T^4, \quad (28)$$

$$s(T) = \frac{2\pi^2}{45} g_{*s}(T) T^3, \quad (29)$$

Here $g_*(T)$ and $g_{*s}(T)$ can be written in the form of a

summation of the contributions of each species as

$$g_*(T) = \sum_i g_{*,i}(T) \left(\frac{T_i}{T} \right)^4, \quad (30)$$

$$g_{*s}(T) = \sum_i g_{*s,i}(T) \left(\frac{T_i}{T} \right)^3, \quad (31)$$

where $g_{*,i}(T)$ and $g_{*s,i}(T)$ represent the contribution of the i th particle species with mass m_i , degrees of freedom g_i and temperature T_i , and are given by

$$g_{*,i}(T) = g_i \frac{15}{\pi^4} \int_{x_i}^{\infty} \frac{(u^2 - x_i^2)^{\frac{1}{2}}}{e^u \pm 1} u^2 du, \quad (32)$$

$$g_{*s,i}(T) = g_i \frac{15}{\pi^4} \int_{x_i}^{\infty} \frac{(u^2 - x_i^2)^{\frac{1}{2}}}{e^u \pm 1} \left(u^2 - \frac{x_i^2}{4} \right) du. \quad (33)$$

For this expression, we define $x_i \equiv m_i/T$ and $u \equiv E_i/T$, where $E_i = \sqrt{|\mathbf{p}_i|^2 + m_i^2}$, and assume that the chemical potential is negligible. The sign $+$ in the denominator denotes fermions and $-$ denotes bosons.

With the help of entropy conservation, $sa^3 = \text{const.}$, Eqs.(28) and (29) lead to $\rho \propto g_* g_{*s}^{-4/3} a^{-4}$. This means the behavior of the Hubble rate in the radiation dominated era is modified as $H \propto g_*^{1/2} g_{*s}^{-2/3} a^{-2}$. Let us briefly consider how the changes in g_* and g_{*s} affect the spectrum of the gravitational wave background. Referring back to the discussion at the end of Sec II, the energy spectrum is written as $\Omega_{GW,0} = (k^2/12a_0^2H_0^2)\mathcal{P}_{T,\text{prim}}(a_{\text{hc}}^2/a_0^2)$. Substituting the modified Hubble rate into the relation $k = a_{\text{hc}}H_{\text{hc}}$, we obtain $a_{\text{hc}} \propto g_{*,\text{hc}}^{1/2} g_{*s,\text{hc}}^{-2/3} k^{-1}$. This leads to $\Omega_{GW,0} \propto g_{*,\text{hc}}^{-1/3} k^0$, where we assume $g_* = g_{*s}$, which holds before the neutrino decoupling, for simplicity. Therefore, since g_* is large at the early stage of the universe when the temperature is high enough for particles to be relativistic, the spectrum is suppressed at the higher frequencies which enter the horizon earlier.

Taking into account the improved evolution of the energy density, the Friedmann equation for the Hubble rate can be expressed in terms of the density parameters as

$$H = H_0 \left[\left(\frac{g_*}{g_{*0}} \right) \left(\frac{g_{*s}}{g_{*s0}} \right)^{-\frac{4}{3}} \Omega_r \left(\frac{a}{a_0} \right)^{-4} + \Omega_m \left(\frac{a}{a_0} \right)^{-3} + \Omega_\Lambda \right]^{\frac{1}{2}}, \quad (34)$$

where Ω_r , Ω_m , and Ω_Λ are the density parameters for radiation, matter and dark energy, respectively. Throughout this paper, we adopt $\Omega_r h^2 = 4.31 \times 10^{-5}$ and the WMAP cosmological parameters $h = 0.732$, $\Omega_m = 0.241$, and $\Omega_\Lambda = 0.759$ [40]. The particles we assume are listed in Table I of Ref. [22]. Here, we consider only particles in the standard model and do not include SUSY particles or any other exotic particles. Including SUSY particles would double g_* at above the TeV scale and $\Omega_{GW,0}(\propto g_{*,\text{hc}}^{-1/3})$ would decrease by a factor of $2^{-1/3} \simeq 0.8$ [41].

IV. SPECTRUM OF PRIMORDIAL GRAVITATIONAL WAVES FROM INFLATION

Before showing our numerical results, we briefly describe details of the numerical calculation method. We first compute the background equations for the Hubble rate using the procedure described in Sec III, and then substitute it into the evolution equation of gravitational waves, Eq.(4), presented in Sec II. Note that this equation is obtained by neglecting the anisotropic stress term, which can be set to zero when neutrinos do not induce an anisotropic stress. We take into account the contribution of the neutrino anisotropic stress by using Eq.(C1) after the time of neutrino decoupling.

For the calculation of the Hubble rate, we use Eqs. (24),(25) and (26) during inflation and reheating. Then we switch to Eq. (34) at the point when the universe becomes well dominated by radiation, $H \propto a^{-2}$. The e-folding number of inflation, corresponding to the pivot scale, is chosen in order to ensure smooth connection to the present Hubble rate. We obtain its exact value by iteratively solving the equations for inflation and reheating.

We start the calculation for each gravitational-wave mode from a point where the mode is well inside the horizon. The initial condition of the mode is set to oscillate with the amplitude given in Eq. (5). Then we solve the evolution of the gravitational waves for each mode using Eq. (2) and the evolution of the Hubble rate. After the mode has re-entered into the horizon and again begun to oscillate rapidly, we replace its evolution with the WKB solution of Eq.(7) since it would be time consuming to treat the oscillations numerically. Note that we also use the WKB solution even when the neutrino anisotropic stress is taken into account because the effect is negligible if $k \gg aH$ (see Appendix C). Finally, we compute the spectrum according to Eq.(8).

A. Chaotic inflation

First, we consider the case where the scalar field has a quadratic potential,

$$V(\phi) = \frac{1}{2}m^2\phi^2. \quad (35)$$

We used the normalization of the scalar perturbations which is derived by combining the constraints from recent observations [42],

$$\mathcal{P}_{S,\text{prim}}(k_{\text{pivot}} = 0.05\text{Mpc}^{-1}) = (2.45 \pm 0.23) \times 10^{-9}. \quad (36)$$

This fixes the value of the scalar field mass to be $m = 1.64 \times 10^{13}\text{GeV}$. The decay rate is set to be $\Gamma = 10^{-2}m$.

Figure 1 shows the result of our numerical calculation. In the lower frequency region, we see a well-known characteristics of the spectrum as described in Sec.II – that is the change of the frequency dependence of the spectrum

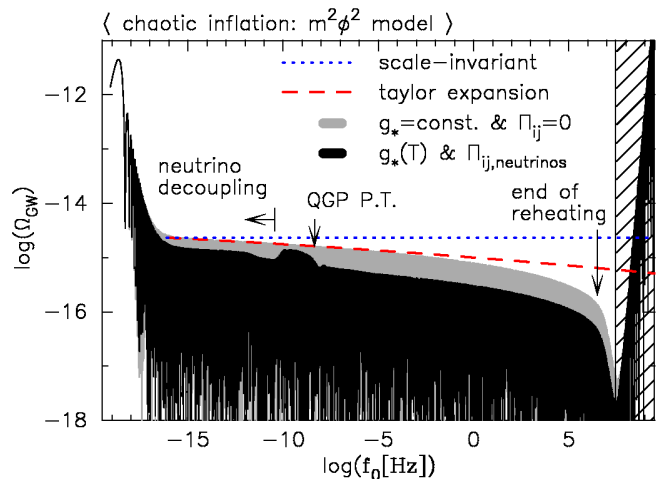


FIG. 1: The spectrum of the gravitational wave background generated during inflation with a quadratic potential $V = m\phi^2/2$, versus the gravitational frequency $f_0 = k/2\pi[\text{Hz}]$. The black-line spectrum includes the effects of g_* changes and the neutrino anisotropic stress, and the light gray one does not. Two lines are shown to compare our numerical result with theoretical prediction: the dotted curve represents a scale-invariant spectrum and the dashed line is the spectrum predicted under the slow-roll approximation, which is plotted according to Eq.(22) with the spectral index $n_T(k_{\text{pivot}}) = -1.76 \times 10^{-2}$ and its running $\alpha_T(k_{\text{pivot}}) = -3.11 \times 10^{-4}$. The shaded area corresponds to the spectrum due to quantum zero point fluctuations (see Sec. IV A).

($\Omega_{\text{GW}} \propto k^{-2}$ to k^0) at around 10^{-17}Hz , which corresponds to the horizon scale at matter-radiation equality. At frequencies above 10^{-17}Hz , the spectrum shows some interesting structural features, which we will focus on for the remainder of this paper.

Let us first discuss the effect of inflation by paying attention to the tilt of the spectrum. For comparison with previous works, we plotted the Taylor-expanded spectrum derived in the slow-roll regime (Eq.(22)). Note that, when comparing with the spectrum of $g_* = \text{const.}$ and $\Pi_{ij} = 0$, our calculation is in good agreement around the pivot wavenumber $k_{\text{pivot}} = 0.05\text{Mpc}^{-1}$ which corresponds to $f_0 \simeq 10^{-16.1}\text{Hz}$. On the other hand, we see deviations from the Taylor-expanded spectrum at frequencies above about 10^{-5}Hz , which includes the frequency bands of LISA [12] and DECIGO/BBO [13, 14]. This is because the Taylor expansion around the pivot scale ($f_{\text{pivot}} \simeq 10^{-16.1}\text{Hz}$) is no longer valid. This can be avoided if one uses Eq.(19) instead of Eq.(22) as long as the slow-roll condition is satisfied. However, at frequencies above 10^6Hz , where one finds the deviation becomes much larger, the slow-roll condition is no longer satisfied. This causes a deviation from the correct amplitude, and is unavoidable in the slow-roll regime. Therefore, the slow-roll approximation overestimates the amplitude of the spectrum at very high frequencies. Moreover, the use of the Taylor-expanded form of the slow-roll approxima-

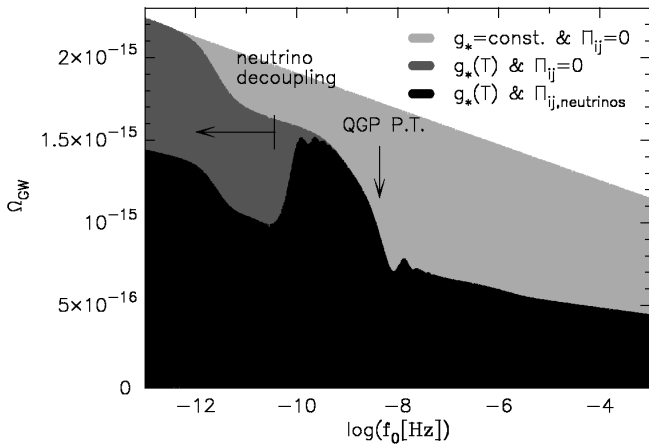


FIG. 2: Portion of the same spectrum of Fig. 1, focusing on the features induced by the change of g_* and the neutrino anisotropic stress. Note that Ω_{GW} is plotted on a linear scale. The black spectrum includes both contributions, the gray one includes only the effect of g_* changes, and the light gray one does not include either.

tion, which is used widely in previous works, makes the deviation larger and also increases the frequency range over which it occurs. Obviously, these deviations are also present when the change of g_* is taken into account.

Other characteristic features in the spectrum are produced after the end of inflation. When comparing with the spectrum which does not include g_* changes and the neutrino anisotropic stress, we find these two effects cause damping over wide frequencies. While the changes of g_* produce damping of higher frequencies (above 10^{-12}Hz) as explained in Sec. III C, the neutrino anisotropic stress mainly causes damping at lower frequencies (10^{-17}Hz to 10^{-10}Hz). At frequencies where the two effects overlap, the spectrum shows features produced by a combination of both the change of g_* and the neutrino anisotropic stress. We present a close-up of the overlapped region in Fig. 2. Note that we additionally show the spectrum which only includes the effect of g_* changes to make it clear which effect causes the damping at each frequency. It may be seen that the stepwise changes of g_* induce a step-like shape in the spectrum and the neutrino anisotropic stress only affects the modes which re-enter the horizon after the time of their decoupling at 2MeV . The magnitude of the damping due to neutrino anisotropic stress may be derived analytically to be 35.6% [21]. Note that our result does not show the dip and peak around $f_0 = 0.8 \times 10^{-10}\text{Hz}$ ($k_0 = 5 \times 10^{-10}\text{Hz}$) as seen in the results of Ref. [22]. We find that the feature does not arise for the reason given in Appendix D of Ref [22], but instead is the result of inaccurate treatment of the source term. For detail, see Appendix B. ²

² We thank Y. Watanabe (private communication) for helping

The change of the Hubble rate produces features in the spectrum around the frequency of the mode that re-enters the horizon at the time of the change. One can relate the frequencies today to the temperature of the universe at the time when the modes re-enter the horizon as [43]

$$f_0 = 1.65 \times 10^{-7} \times \frac{1}{2\pi} \times \left[\frac{T_{\text{hc}}}{1\text{GeV}} \right] \left[\frac{g_{*s}(T_{\text{hc}})}{100} \right]^{-\frac{1}{3}} \left[\frac{g_*(T_{\text{hc}})}{100} \right]^{\frac{1}{2}} \text{Hz}. \quad (37)$$

For example, substituting the temperature of the QGP phase transition, which is assumed to occur at 180MeV , for T_{hc} yields $f_0 \simeq 10^{-8}\text{Hz}$. Indeed, at around this frequency, we do find the large step due to the sudden change of g_* [22]. Also, the change of the frequency dependence ($\Omega_{\text{GW}} \propto k^0$ to k^{-2}) at around $f_0 \simeq 10^7\text{Hz}$ corresponds to the reheating temperature $T_{\text{RH}} \simeq 2 \times 10^{14}\text{GeV}$, which is derived by substituting $\Gamma = 10^{-2}m \simeq 10^{11}\text{GeV}$ into Eq.(27). It is notable that the k^{-2} dependence above 10^7Hz is the reheating effect due to the fact that the Hubble rate has the same evolution as a matter-dominated universe during reheating.

One thing we have to mention here is the significant rise at the highest frequencies, which is proportional to k^4 . These are the modes which have not crossed outside the horizon during inflation, so that their amplitude decrease as $\Omega_{\text{GW}} \propto a^{-2}$ all the way through keeping the gradient of the initial spectrum. Of course they may not in truth exist because they do not "freeze in" as classical fluctuations. One may regard them not as gravitational waves which have been propagating since the epoch of inflation, but as quantum perturbations of the space-time metric which are arising "just now". ³

B. Low reheating temperature

Here, we consider different reheating temperatures, referring to the upper bound from the gravitino problem, $T_{\text{RH}} < 10^6 - 10^9\text{GeV}$ [44]. As we discussed in the previous subsection, the reheating temperature determines the characteristic frequency of the feature induced by reheating, so that different reheating temperatures are expected to result in different spectrum shapes. Here, we consider the case of $T_{\text{RH}} = 10^9\text{GeV}$ and 10^6GeV , which corresponds to the decay rate $\Gamma \simeq 2 \times 10^{-11}m$ and $2 \times 10^{-17}m$.

to clarify the reason for the difference between our results and theirs.

³ These modes are considered to be contributing to the cosmological constant and tuned to be very small. However, for reference, if they contribute to the total energy density of the universe, the energy density of the gravitational waves exceeds that of the scalar field for $f_0 \gtrsim 10^{11}\text{Hz}$, and the linear analysis becomes invalid.

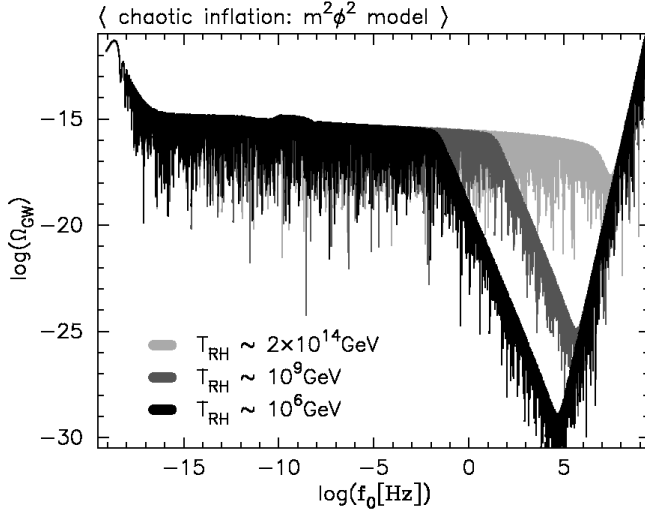


FIG. 3: The spectrum for different values of the reheating temperature for chaotic inflation. The lightest gray spectrum is the same as shown in Fig. 1, i.e. the decay rate is set to be $\Gamma = 10^{-2}m$ which corresponds to $T_{\text{RH}} \simeq 2 \times 10^{14} \text{ GeV}$. The dark gray one shows the case of $T_{\text{RH}} \simeq 10^9 \text{ GeV}$ and the black one shows the case of $T_{\text{RH}} \simeq 10^6 \text{ GeV}$.

The calculation is carried out with the same condition as that of quadratic chaotic inflation except the value of the decay rate.

Shown in Fig. 3 is a comparison of the spectrum at different reheating temperatures. It can be seen that each spectrum has the k^{-2} dependence due to the reheating effect, although their length are quite different. This is because a lower decay rate makes the reheating time longer. Note that the edge at the frequency which corresponds to the reheating temperature shifts to lower frequencies as the reheating temperature decreases. This behavior is consistent with the estimation from Eq.(37) that the corresponding frequencies for $T_{\text{RH}} = 10^6 \text{ GeV}$ and 10^9 GeV are 10^{-2} Hz and 10^1 Hz which will be covered by DECIGO/BBO. It is an exciting possibility to determine the reheating temperature of the universe by these experiments [45, 46].

C. Application to other inflation models

We also repeat the calculations for other inflation models: $\lambda\phi^4$, new inflation, and hybrid inflation. In each case, we adopt the same normalization as in Eq.(36) and set the decay rate to be $\Gamma = 10^{-2}\bar{m}$, where \bar{m} is the effective mass of the scalar field at the minimum of the potential. The results for each model are summarized in Fig. 4. The values of n_T , α_T , which are required to draw a line of the slow-roll prediction, and r are listed in Table I. Also, the comparison between all models is shown in Fig. 5.

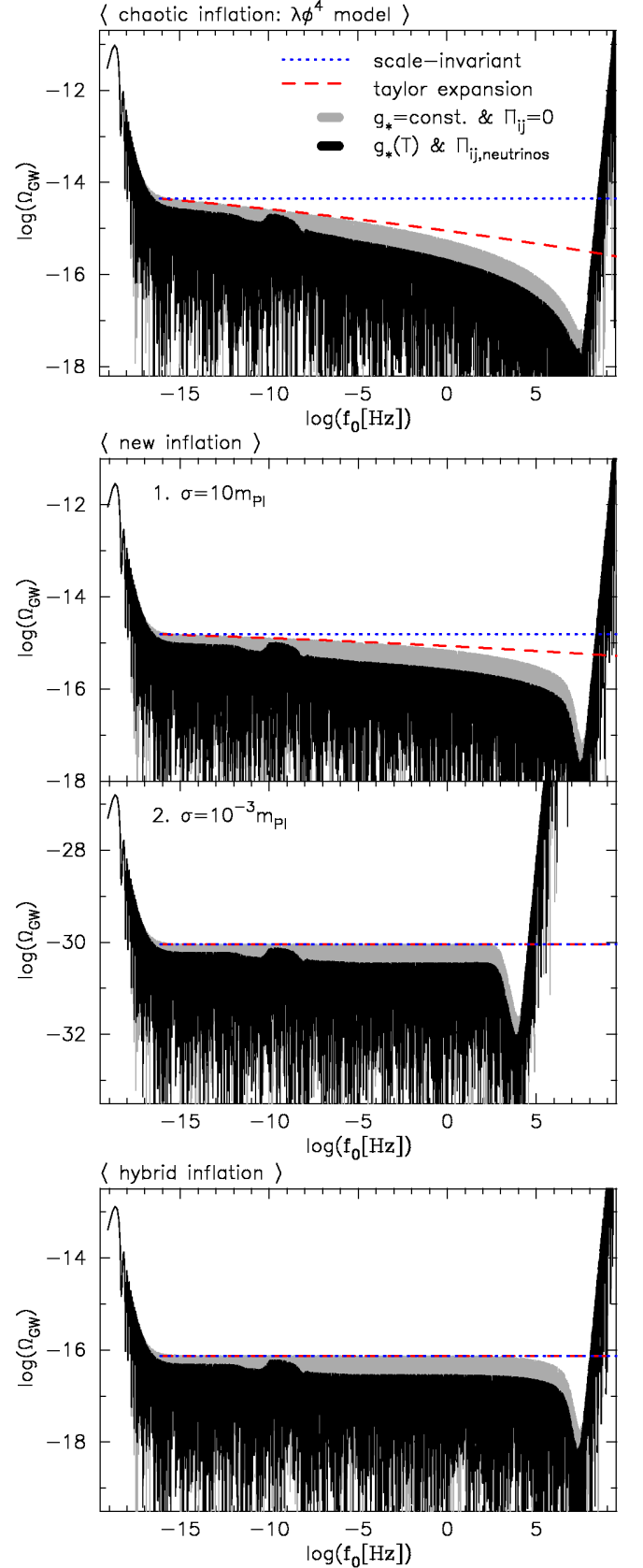


FIG. 4: The spectrum for different inflation potentials.

1. $\lambda\phi^4$ model

Let us consider chaotic inflation with a quartic potential,

$$V(\phi) = \frac{1}{4}\lambda\phi^4, \quad (38)$$

where the normalization gives $\lambda = 1.78 \times 10^{-13} \text{GeV}$. A notable characteristic of this type of potential is that the decay rate is not constant, because the oscillation frequency of ϕ depends on the amplitude of ϕ , i.e. $\bar{m} = c\sqrt{\lambda}\langle\phi\rangle$, where c is a constant of order 1 [47, 48].

In the ϕ^4 case, the Hubble rate behaves as in a radiation-dominated universe when the ϕ field oscillates about the minimum of the potential. Indeed, as one can find from the spectrum at the top of Fig. 4, there is no matter-dominated phase (k^{-2} dependence) soon after inflation. Therefore, for ϕ^4 model, we cannot distinguish the stage of reheating and the subsequent radiation-dominated era, so that the uncertainty of the decay rate does not affect the resultant spectrum at all. Note that the large gap at high frequencies is only because of the large deviation from the slow-roll approximation, which is also an interesting characteristic of this potential. Again, as is seen from the figure, the Taylor-expanded spectrum overestimates the spectrum at $f_0 \gtrsim 10^{-5} \text{ Hz}$.

2. new inflation

We now consider the original new inflation model which is based on the Coleman-Weinberg potential [49],

$$V(\phi) = \frac{1}{4}\lambda\phi^4 \left(\ln \frac{\phi}{\sigma} - \frac{1}{4} \right) + \frac{\lambda\sigma^4}{16}. \quad (39)$$

The oscillation frequency is given by $\bar{m} = \sigma\sqrt{\lambda}$. Here, we present the results for two different parameter sets: (1) $\sigma = 10m_{Pl}$, $\lambda = 2.36 \times 10^{-14} \text{GeV}$ and (2) $\sigma = 10^{-3}m_{Pl}$, $\lambda = 7.27 \times 10^{-12} \text{GeV}$. In case (1), we find a very similar spectrum to the case of the $m^2\phi^2$ potential. By contrast, in case (2), the spectrum is quite different. This difference arises from the difference in the point in the potential at which the ϕ field rolls down. In case (1), the scalar field rolled down where the potential is quadratic, and this is why the spectrum has almost the same shape as that of the $m^2\phi^2$ case.

In case (2), inflation occurs at a lower energy scale, and the decay rate is set to be smaller, $\Gamma = 10^{-6}\bar{m}$, in order to not exceed the Hubble rate during inflation. The remarkable features of case (2) are the complete flatness of the spectrum and the smallness of its amplitude. The flatness is due to the small gradient of the potential because the initial value of ϕ is very near zero. The smallness of the amplitude relates to the flatness of the spectrum, about which we will explain later.

Model	n_T	α_T	r
$m^2\phi^2$	-1.76×10^{-2}	-3.11×10^{-4}	0.141
$\lambda\phi^4$	-3.40×10^{-2}	-5.78×10^{-4}	0.272
new (1)	-1.16×10^{-2}	-2.60×10^{-4}	9.31×10^{-2}
new (2)	-6.83×10^{-18}	-4.77×10^{-19}	5.47×10^{-17}
hybrid	-5.80×10^{-4}	3.30×10^{-6}	4.64×10^{-3}

TABLE I: A summary of the values of the inflationary parameters n_T , α_T , and r for each model. These are evaluated at $k_{\text{pivot}} = 0.05 \text{Mpc}^{-1}$.

3. hybrid inflation

In the case of hybrid inflation, the potential is constructed with two scalar fields ϕ and σ [50, 51],

$$V(\phi) = \frac{1}{4\lambda}(M^2 - \lambda\sigma^2)^2 + \frac{1}{2}m^2\phi^2 + \frac{1}{2}g^2\phi^2\sigma^2. \quad (40)$$

We consider the usual case where inflation is driven by the ϕ field and suddenly ends after the symmetry breaking of the σ field (waterfall field). To satisfy this condition, we adopt the following parameters: $\lambda = 1$, $g = 8 \times 10^{-4}$, $m = 1.5 \times 10^{-7}m_{Pl}$, $M = 1.21 \times 10^{16} \text{GeV}$. In this case, the oscillation at the bottom of the potential mainly comes from the ϕ field, of which the frequency is $\bar{m}_\phi = gM/\sqrt{\lambda}$, thus we can assume that the radiation energy produced during reheating comes from only the decay of the ϕ field.

The spectrum shown at the bottom of Fig. 4 is nearly flat and in good agreement with the Taylor-expanded spectrum. This is because the quite gentle slope of the potential of the ϕ field results in an almost constant value of the Hubble rate as long as the σ field triggers the sudden end of inflation. Thus, the spectrum has less frequency dependence, which leads to less deviation from the Taylor expansion. Also, interestingly, the value of α_T is positive, which means $\eta > 2\epsilon$. Both of these are the specific features of hybrid inflation.

4. Comparison

Finally, in Fig.5, we compare all models. In each case, the effects of neutrino anisotropic stress and the g_* changes appear of course in the same way at the same position because these shapes are formed well after the end of inflation. Needless to say, the differences between the models arise due to the difference in how the scalar field evolves in each potential during inflation. The behavior of the Hubble rate during reheating is also important as a model dependent factor. Indeed, the reason for the unique shape of the $\lambda\phi^4$ model at high frequencies is because the Hubble rate evolves differently than the other three models.

	$10^{-16.1}\text{Hz}$	10^{-5}Hz	10^{-3}Hz	10^{-1}Hz	10^2Hz	$\text{SNR}/\sqrt{T_{\text{obs}}/10\text{yr}}$
chaotic ($m^2\phi^2$)						
$g_*(T) \& \Pi_{ij,\text{neutrinos}}$	1.77×10^{-15}	4.90×10^{-16}	4.14×10^{-16}	3.39×10^{-16}	2.27×10^{-16}	4.80
$g_* = \text{const.} \& \Pi_{ij} = 0$	2.57×10^{-15}	1.26×10^{-15}	1.07×10^{-15}	8.79×10^{-16}	5.92×10^{-16}	12.0
Taylor-expanded slow-roll	–	1.35×10^{-15}	1.21×10^{-15}	1.07×10^{-15}	8.80×10^{-16}	15.2
chaotic ($m^2\phi^2$, $T_{\text{RH}} = 10^9\text{GeV}$)						
$g_*(T) \& \Pi_{ij,\text{neutrinos}}$	2.75×10^{-15}	4.90×10^{-16}	4.01×10^{-16}	3.17×10^{-16}	9.12×10^{-18}	4.53
chaotic ($m^2\phi^2$, $T_{\text{RH}} = 10^6\text{GeV}$)						
$g_*(T) \& \Pi_{ij,\text{neutrinos}}$	2.88×10^{-15}	4.90×10^{-16}	3.94×10^{-16}	1.51×10^{-17}	7.60×10^{-24}	0.20
chaotic ($\lambda\phi^4$)						
$g_*(T) \& \Pi_{ij,\text{neutrinos}}$	3.47×10^{-15}	5.37×10^{-16}	3.85×10^{-16}	2.65×10^{-16}	1.24×10^{-16}	3.66
$g_* = \text{const.} \& \Pi_{ij} = 0$	5.01×10^{-15}	1.38×10^{-15}	1.00×10^{-15}	6.93×10^{-16}	3.27×10^{-16}	9.46
Taylor-expanded slow-roll	–	1.58×10^{-15}	1.27×10^{-15}	1.01×10^{-15}	6.99×10^{-16}	14.2
new inflation ($\sigma = 10m_{\text{pl}}$)						
$g_*(T) \& \Pi_{ij,\text{neutrinos}}$	1.20×10^{-15}	3.89×10^{-16}	3.40×10^{-16}	2.91×10^{-16}	2.09×10^{-16}	4.36
$g_* = \text{const.} \& \Pi_{ij} = 0$	1.70×10^{-15}	1.00×10^{-15}	8.81×10^{-16}	7.55×10^{-16}	5.47×10^{-16}	11.0
Taylor-expanded slow-roll	–	1.07×10^{-15}	9.77×10^{-16}	8.95×10^{-16}	7.78×10^{-16}	14.7
new inflation ($\sigma = 10^{-3}m_{\text{pl}}$)						
$g_*(T) \& \Pi_{ij,\text{neutrinos}}$	7.08×10^{-31}	3.55×10^{-31}	3.54×10^{-31}	3.54×10^{-31}	3.51×10^{-31}	4.95×10^{-15}
$g_* = \text{const.} \& \Pi_{ij} = 0$	1.00×10^{-30}	9.02×10^{-31}	9.01×10^{-31}	9.01×10^{-31}	8.97×10^{-31}	1.27×10^{-14}
Taylor-expanded slow-roll	–	9.02×10^{-31}	9.02×10^{-31}	9.02×10^{-31}	9.02×10^{-31}	2.58×10^{-14}
hybrid inflation						
$g_*(T) \& \Pi_{ij,\text{neutrinos}}$	5.75×10^{-17}	2.88×10^{-17}	2.85×10^{-17}	2.84×10^{-17}	2.77×10^{-17}	0.41
$g_* = \text{const.} \& \Pi_{ij} = 0$	8.32×10^{-17}	7.41×10^{-17}	7.38×10^{-17}	7.36×10^{-17}	7.18×10^{-17}	1.02
Taylor-expanded slow-roll	–	7.41×10^{-17}	7.38×10^{-17}	7.36×10^{-17}	7.34×10^{-17}	1.05

TABLE II: The density parameter of gravitational wave background Ω_{GW} at $f_0 = 10^{-16.1}, 10^{-5}, 10^{-3}, 10^{-1}, 10^2\text{Hz}$ for several inflation models, (1) calculated by fully numerically solving the evolution of gravitational waves including g_* change and the neutrino isotropic stress, or (2) assuming $g_* = \text{const.} \& \Pi_{ij} = 0$, or (3) estimated by the Taylor-expanded form of the slow-roll approximation using Eq.(22) with $g_* = \text{const.} \& \Pi_{ij} = 0$. In addition, the rightmost column shows the signal-to-noise ratios for DECIGO, which is aimed at 10^{-1}Hz .

Note that the flatter the spectrum, the more the amplitude of large-scale modes is suppressed. This behavior can be explained as follows: From Eq. (23), one can easily find $\mathcal{P}_{T,\text{prim}} = r\mathcal{P}_{S,\text{prim}}$. Since we normalize the amplitude of the spectrum using the value of $\mathcal{P}_{S,\text{prim}}$, the smaller scalar tensor ratio r results in a smaller amplitude of the primordial gravitational wave spectrum. In addition, r can be rewritten as $r \simeq -8n_T$, the tilt of the spectrum. This is equivalent to saying that a flatter spectrum leads to a smaller amplitude primordial gravitational wave spectrum. This can be confirmed by comparing the values of r or n_T given in Table I with the spectrum amplitudes at the pivot scale (see the case of $g_* = \text{const.}$ and $\Pi_{ij} = 0$), presented in the first column of Table II. The extremely tiny value of r in new inflation case (2) is the reason why the amplitude of the spectrum

in that case is quite small.

We also provide in Table II the detailed numerical values of the spectrum at $f_0 = 10^{-5}, 10^{-3}, 10^{-1}, 10^2\text{Hz}$ (including the frequency bands of LISA [12], DECIGO/BBO [13, 14] and LIGOII/LCGT [15, 16]) for several inflation models. For comparison, the values of Ω_{GW} , calculated assuming $g_* = \text{const.}$ and $\Pi_{ij} = 0$ or using the Taylor-expanded spectrum predicted under the slow-roll approximation, Eq.(22), are also given. These clearly illustrate the suppression of the precise values compared to those derived under these assumptions. For reference, we calculate the predicted signal-to-noise ratio (SNR) using the noise spectrum of DECIGO, which assumes a Fabry-Perot type space interferometer and ten years of observing time ($T_{\text{obs}} = 10\text{yr}$) [41, 52]. This is shown in the rightmost column in Table II. Note that we find large

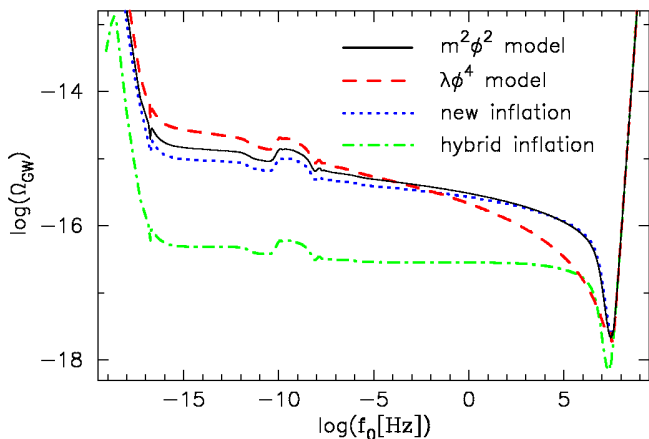


FIG. 5: The spectrum of gravitational wave background is shown for several inflation models. The solid curve shows the spectrum for the quadratic potential, the dashed curve for the quartic potential, the dotted curve for the new inflation potential with $\sigma = 10m_{Pl}$, and dot-dash curve for hybrid inflation.

differences in SNR between results from the spectrum we have obtained and the Taylor-expanded spectrum. This clearly illustrates the reason why it is necessary to evaluate the spectrum amplitude numerically. We find that the damping effect due to the changes of g_* decreases the SNR dramatically, and also the assumption of the Taylor-expanded slow-roll overestimates the SNR in some cases. The difference is more prominent for the models with steeper potential such as chaotic inflation models. A detailed analysis of the detectability will be done using the results of this paper in our future work.

V. CONCLUSION

Gravitational waves generated during inflation are expected to be a powerful tool to probe the physics of the early universe. In particular, direct detection of gravitational waves would provide vital information on their high frequency modes. In this paper, we have calculated the spectrum of the gravitational wave background over a wide range of frequencies (from 10^{-19} to 10^8 Hz) including the very high frequencies where we expect to see a deviation from the slow-roll approximation and the effect of reheating. This has become possible by numerically solving the evolution of a scalar field from quantum states during inflation until today taking into account the conversion of the scalar field energy into radiation. In addition, we have also taken into account the contribution of neutrinos to the anisotropic stress and the temperature dependence of the effective degrees of freedom g_* . These two effects had already been investigated by Ref. [22]. However, we found that a correction is needed for the treatment of the source term in their calculation. Moreover their calculation is limited in terms of frequency range, so that their

result is not relevant to the reheating process. Therefore, this is the first calculation that correctly includes all the factors which affect the shape of the gravitational wave background spectrum over a wide range of frequencies. This comprehensive treatment of the factors enables us to make an accurate estimation of the amplitude of the spectrum, which should be invaluable in making predictions for future experiments.

Our estimation shows that the Taylor-expanded spectrum of the slow-roll prediction Eq. (22), which is analytically obtained and used in many previous works, overestimates the amplitude of the spectrum in some models. The deviation between our result and the analytical prediction is especially evident at high frequencies ($f_0 \gtrsim 10^6$ Hz) because the slow-roll conditions are violated towards the end of inflation. It is also notable that the deviation is found even in the frequency region where the slow-roll conditions are satisfied (around between 10^5 Hz and 10^{-6} Hz in the $m^2\phi^2$ case). This is because the Taylor expansion of the spectrum around the CMB scale is no longer a good approximation at these frequencies. However, since we do not know the normalization of the scalar perturbations at much smaller scales ($< \text{kpc}$), it is impossible to carry out a Taylor expansion about a high frequency point. Therefore the deviation is inevitable as long as we analytically evaluate the spectrum using the Taylor expansion as in Eq. (22). We strongly recommend numerical calculation of spectra in order to discuss the detectability of the gravitational wave background.

Moreover, we have shown that the spectrum has the characteristic features produced after the end of inflation. The effect of reheating is observed in the spectrum as a dip at $\sim 10^8$ Hz in the case where the scalar field oscillates in a quadratic-like potential. This is because the matter-dominated evolution of the universe during reheating causes the frequency dependence of k^{-2} . This feature is not seen in the case of a quartic potential because of the difference in the evolution of the Hubble rate. In addition, the combination of the effects due to changes in g_* and the neutrino anisotropic stress is observed between 10^{-17} – 10^{-6} Hz. It should be noted that changes in g_* decrease the amplitude by about half an order of magnitude at higher frequencies, where the above-mentioned features of the early universe notably appear. This damping effect becomes larger in case where there exist SUSY particles or other exotic particles which cause a change of g_* [22]. We have confirmed that this effect is also important when evaluating the detectability.

Finally, we would like to conclude with some prospects for future observations. When comparing the results of different inflation models, we found that the amplitudes of the three models, both cases of chaotic inflation and case (1) new inflation, are comparable around the frequencies covered by future experiments like LISA, DECIGO/BBO and LIGOII/LCGT. Thus, to distinguish these models, it may be necessary to measure the tilt of the spectrum. Furthermore, interestingly, the frequencies

covered by future experiments cover the range in which the spectrum shows an edge due to the effect of the low temperature reheating. Hopefully, they will provide a new insight into understanding of reheating.

Also, high frequency gravitational wave background around 10^8Hz , which the new design of detector suggested in Ref. [17] is targeting, will be a probe of reheating process soon after inflation. This is also the frequency at which we found the connecting point to the k^4 dependence, beyond which the waves are considered to not "freeze in" as classical fluctuations. However, the mechanism of "freeze in" is yet to be uncovered. Therefore, through future direct detection at around 10^8Hz , we may obtain information not only on reheating but also on classicalization of the quantum fluctuations.

Acknowledgments

The authors are grateful to Takayuki Kaku for his contribution at the early stage of this work, to Yuki Watanabe for useful correspondence, and to Joanne Dawson for careful correction of the manuscript. T.C. would like to thank Jun'chi Yokoyama for useful discussion. This research is supported by Grant-in-Aid for Nagoya University Global COE Program, "Quest for Fundamental Principles in the Universe: from Particles to the Solar System and the Cosmos", and Grant-in-Aid for Scientific Research on Priority Areas No. 467 "Probing the Dark Energy through an Extremely Wide and Deep Survey with Subaru Telescope", from the Ministry of Education, Culture, Sports, Science and Technology of Japan. Also, this work was supported in part by Grant-in-Aid for Scientific Research from JSPS (No.17204018(TC and NS) and No.20540280(TC)) and from MEXT (No. 20040006(TC)) and in part by Nihon University.

APPENDIX A: QUANTIZATION OF TENSOR PERTURBATIONS

To describe the initial condition of gravitational waves during inflation, we need a quantum-mechanical treatment. Here, we do not go into details but give a brief description of how to proceed (For details, see Ref. [23, 29]).

The quantization is carried out by introducing the rescaled variable $v_{\mathbf{k}}^{\lambda}(\tau, \mathbf{k}) \equiv ah_{\mathbf{k}}^{\lambda}/\sqrt{16\pi G}$ which satisfies the commutation relations with its momentum $\pi_{\mathbf{k}}^{\lambda}(\tau, \mathbf{k}) = \partial v_{\mathbf{k}}^{\lambda}(\tau, \mathbf{k})/\partial\tau$,

$$\begin{aligned} [\hat{v}_{\mathbf{k}}^{\lambda}, \hat{\pi}_{\mathbf{l}}^{\sigma\dagger}] &= i\delta^{\lambda\sigma}\delta^{(3)}(\mathbf{k}-\mathbf{l}), \\ [\hat{v}_{\mathbf{k}}^{\lambda}, \hat{v}_{\mathbf{l}}^{\sigma}] &= [\hat{\pi}_{\mathbf{k}}^{\lambda\dagger}, \hat{\pi}_{\mathbf{l}}^{\sigma\dagger}] = 0. \end{aligned} \quad (\text{A1})$$

We take the expression for the quantum operator

$$\hat{v}_{\mathbf{k}}^{\lambda}(\tau, \mathbf{k}) = v_k(\tau, k)\hat{a}_{\mathbf{k}}^{\lambda} + v_k^*(\tau, k)\hat{a}_{-\mathbf{k}}^{\lambda\dagger}, \quad (\text{A2})$$

where the creation and annihilation operators, $\hat{a}_{\mathbf{k}}^{\lambda}$ and $\hat{a}_{-\mathbf{k}}^{\lambda\dagger}$, satisfy the commutation relations

$$\begin{aligned} [\hat{a}_{\mathbf{k}}^{\lambda}, \hat{a}_{\mathbf{l}}^{\sigma\dagger}] &= \delta^{\lambda\sigma}\delta^{(3)}(\mathbf{k}-\mathbf{l}), \\ [\hat{a}_{\mathbf{k}}^{\lambda}, \hat{a}_{\mathbf{l}}^{\sigma}] &= [\hat{a}_{\mathbf{k}}^{\lambda\dagger}, \hat{a}_{\mathbf{l}}^{\sigma\dagger}] = 0. \end{aligned} \quad (\text{A3})$$

This follow from the Wronskian condition

$$v_k^* \frac{dv_k}{d\tau} - v_k \frac{dv_k^*}{d\tau} = -i. \quad (\text{A4})$$

Then Eq. (2) can be recast in terms of conformal time derivatives as

$$\frac{d^2 v_k}{d\tau^2} + \left(k^2 - \frac{1}{a} \frac{d^2 a}{d\tau^2} \right) v_k = 0. \quad (\text{A5})$$

Using the relation between the conformal time and the expansion rate during inflation, $\tau \simeq -1/(aH)$ which is equivalent with $da/d\tau \simeq -a/\tau$, the second derivative term can be rewritten as $(d^2 a/d\tau^2)/a \simeq 2/\tau^2$. When considering the short-wavelength limit $k/aH \rightarrow \infty$, we can neglect the term of $1/\tau \simeq -aH$ which is much smaller than the k term, and obtain the asymptotic solution using the normalization of Eq. (A4),

$$v_k \rightarrow \frac{1}{\sqrt{2k}} e^{-ik\tau}. \quad (\text{A6})$$

This is the solution for the modes well inside the horizon during inflation – that is what we set as initial condition in our calculation.

APPENDIX B: THE WKB SOLUTION

Here we present the derivation of the WKB solution, Eq. (7). First, we rewrite Eq. (4) in terms of conformal time τ ,

$$\frac{d^2 h_{\mathbf{k}}^{\lambda}}{d\tau^2} + \left[\frac{2}{a} \frac{da}{d\tau} \right] \frac{dh_{\mathbf{k}}^{\lambda}}{d\tau} + k^2 h_{\mathbf{k}}^{\lambda} = 0. \quad (\text{B1})$$

One may assume the form of the solution as

$$h_{\mathbf{k}}^{\lambda}(\tau) = A(\tau) \exp[iB(\tau)], \quad (\text{B2})$$

and consider the case in which the oscillation is very rapid compared to the time variation of the amplitude, which means $dA/d\tau$ and $d^2 A/d\tau^2$ are much smaller than $dB/d\tau$. By substituting Eq. (B2) into Eq. (B1), we obtain two equations arising respectively from the real part and the imaginary part,

$$\frac{d^2 A}{d\tau^2} - A \left(\frac{dB}{d\tau} \right)^2 + \left[\frac{2}{a} \frac{da}{d\tau} \right] \frac{dA}{d\tau} + k^2 A = 0, \quad (\text{B3})$$

$$2 \frac{dA}{d\tau} \frac{dB}{d\tau} + A \frac{d^2 B}{d\tau^2} + \left[\frac{2}{a} \frac{da}{d\tau} \right] A \frac{dB}{d\tau} = 0. \quad (\text{B4})$$

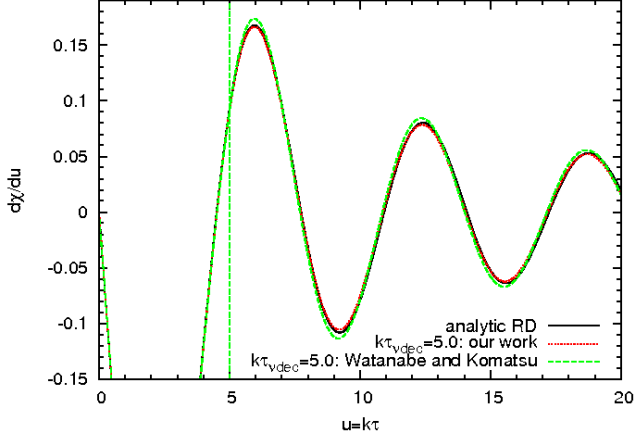


FIG. 6: Time evolution of $\chi'(u \equiv k\tau) \equiv h_{\mathbf{k}}^{\lambda'}(u)/h_{\mathbf{k}}^{\lambda}(0)$ for the mode $k\tau_{\nu,\text{dec}} = 5.0$, which entered the horizon before neutrino decoupling. The solid line is the analytical solution, $\chi' = -j_1(u)$, and does not include the effect of neutrino anisotropic stress. The dotted line, which is almost indistinguishable from the analytical solution, represents our numerical result. The dashed line is an attempt to reproduce the numerical result of Ref. [22]. The vertical dashed line represents the time of neutrino decoupling.

Using the assumption that $d^2A/d\tau^2 \ll dB/d\tau$ and considering the modes well inside the horizon $(da/d\tau)/a \ll k$, we obtain the solution of $B(\tau)$ from Eq. (B3),

$$B(\tau) = \pm k\tau + \text{const.} \quad (\text{B5})$$

The solution of $A(\tau)$ is derived by substituting this into Eq. (B4),

$$A(\tau) \propto a^{-1}. \quad (\text{B6})$$

Therefore we obtain the WKB solution,

$$h_{\mathbf{k}}^{\lambda}(\tau) = \frac{C}{a} \exp(\pm ik\tau + \alpha). \quad (\text{B7})$$

where C and α are arbitrary constants.

APPENDIX C: ANISOTROPIC STRESS OF FREE-STREAMING NEUTRINOS

Analytically solving the linearized Boltzmann equation for neutrinos, we can calculate the spectrum including the effect of free-streaming neutrinos by only evolving $h_{\mathbf{k}}^{\lambda}$. According to Ref. [21] the evolution equation, Eq.(2), can be rewritten in the form of an integro-differential equation with using conformal time τ ,

$$\begin{aligned} \frac{d^2 h_{\mathbf{k}}^{\lambda}(\tau)}{d\tau^2} + \left[\frac{2}{a} \frac{da}{d\tau} \right] \frac{dh_{\mathbf{k}}^{\lambda}(\tau)}{d\tau} + k^2 h_{\mathbf{k}}^{\lambda}(\tau) = -24 f_{\nu}(\tau) \\ \times \left[\frac{1}{a} \frac{da}{d\tau} \right]^2 \int_{\tau_{\nu,\text{dec}}}^{\tau} d\tau' \left[\frac{j_2(k(\tau - \tau'))}{k^2(\tau - \tau')^2} \right] \frac{dh_{\mathbf{k}}^{\lambda}(\tau')}{d\tau}, \quad (\text{C1}) \end{aligned}$$

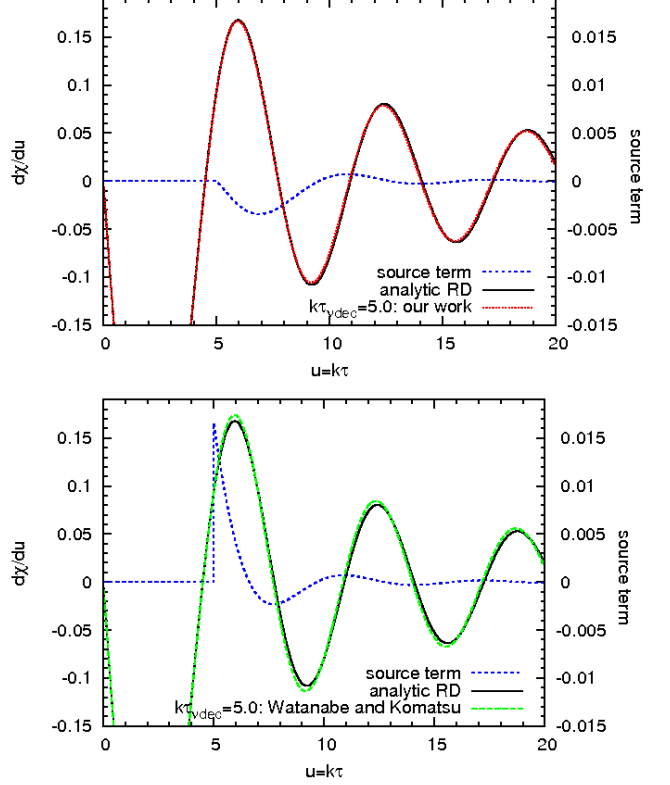


FIG. 7: Evolution of the source term, i.e. the right-hand side of Eq.(C1). The upper figure shows our results and the lower shows the reproduced results of Ref. [22]. The solid, dotted and dashed lines are the same as in Fig 6, and the short-dashed line represents the source term. The artificially introduced discontinuity in the source term in the lower panel has been chosen by trial and error to recover the evolution of Ref. [22]. Note that the scale of the vertical axis for the source term is ten times larger than that for the others.

where j_2 is the spherical Bessel function of order 2. The function $f_{\nu}(\tau)$ describes the fractional energy density of neutrinos, which is defined using the total energy density ρ and the energy density of neutrinos ρ_{ν} as

$$f_{\nu}(\tau) \equiv \frac{\rho_{\nu}(\tau)}{\rho(\tau)} = \frac{f_{\nu,0}}{1 + a(\tau)/a_{\text{eq}}}, \quad (\text{C2})$$

where $f_{\nu,0} = \Omega_{\nu}/(\Omega_{\gamma} + \Omega_{\nu}) = 0.40523$.

Neutrinos do not induce an anisotropic stress at earlier epochs of the universe, because they are in equilibrium with electrons and photons which are coupled to the non-relativistic baryonic matter whose anisotropic stress is negligible. After they decouple and begin free-streaming, their anisotropic stress affects the evolution of the gravitational waves as viscosity. As seen in Eq.(C1), the source term depends on the Hubble rate, which means the anisotropic stress does not affect the mode when it is deep inside the horizon ($k \gg aH$). Thus, the damping effect does not arise at the higher frequency modes which were already inside the horizon at the time of

neutrino decoupling. Also, once the universe becomes matter-dominated, the contribution of neutrinos to the total energy density of the universe becomes sufficiently small ($f_\nu(\tau) \ll 1$), thus the damping effect does not appear in the modes which enter the horizon during the matter-dominated era. Therefore, the damping effect of the neutrino anisotropic stress is seen between the modes which correspond to the time of neutrino decoupling ($f_0 \sim 10^{-10}\text{Hz}$) and radiation-matter equality ($f_0 \sim 10^{-17}\text{Hz}$).

Here, we explain the reason why our spectrum does not have the dip and peak which are seen in the spectrum obtained by Watanabe and Komatsu [22]. In their paper, a small ripple is seen around the frequency corresponding to the time of neutrino decoupling, $f_0 = 0.8 \times 10^{-10}\text{Hz}$ ($k_0 = 5 \times 10^{-10}\text{Hz}$), and is interpreted as a result of assuming instantaneous decoupling. As seen in Fig. 2, our result also shows a ripple at around the same frequency, however it does not show a large dip and peak as observed in their spectrum (see Fig. 5 of Ref. [22]). The detailed reason for the peak is explained in Ref. [22] using a plot of the time evolution of the amplified mode (see Fig. 10 of Ref. [22]). Their suggestion is that the mode gains energy from neutrinos when the derivative

of the mode, $\chi'(u \equiv k\tau) \equiv h_{\mathbf{k}}^{\mathcal{N}}(u)/h_{\mathbf{k}}^\lambda(0)$, is positive, so that it is amplified in the case where the mode enters the horizon when $\chi' > 0$. However, we have reproduced the same behavior by changing the source term, and found that the amplification does not arise for the reason suggested in their paper.

The reproduced behavior of the derivative of the mode is plotted in Fig. 6, which presents the same quantities as Fig. 10 of Ref. [22]. We also plot the result of our calculation in the same figure. Note that the amplification which is seen in the reproduced mode does not appear in our result. This difference is explained by the behavior of the source term, which is presented in Fig. 7. As seen in Fig. 7, the source term has an unnatural discontinuous jump in the case where the mode is amplified. This behavior can be reproduced when we calculate the source term by replacing the lower limit of the integral in Eq. (C1) with zero and switch the source term to affect the evolution of gravitational waves at the time of neutrino decoupling. Therefore the dip and peak seen in Ref. [22] are due to inaccuracy in computing the source term. The validity of our calculation has been confirmed by the author of Ref. [22], Y. Watanabe, via private communication.

-
- [1] A. H. Guth, Phys. Rev. D **23**, 347 (1981).
 - [2] A. Albrecht and P. J. Steinhardt, Phys. Rev. Lett. **48**, 1220 (1982).
 - [3] A. Linde, Phys. Lett. B **108**, 389 (1982).
 - [4] A. H. Guth and S. Y. Pi, Phys. Rev. Lett. **49**, 1110 (1982).
 - [5] A. D. Linde, Phys. Lett. B **116**, 335 (1982).
 - [6] J. M. Bardeen, P. J. Steinhardt, and M. S. Turner, Phys. Rev. D **28**, 679 (1983).
 - [7] B. Allen, Phys. Rev. D **37**, 2078 (1988).
 - [8] V. Sahni, Phys. Rev. D **42**, 453 (1990).
 - [9] L. P. Grishchuk and Y. V. Sidorov, Phys. Rev. D **42**, 3413 (1990); L. P. Grishchuk and M. Solokhin, Phys. Rev. D **43**, 2566 (1991).
 - [10] U. Seljak and M. Zaldarriaga, Phys. Rev. Lett. **78**, 2054 (1997); M. Zaldarriaga and U. Seljak, Phys. Rev. D **55**, 1830 (1997).
 - [11] M. Kamionkowski, A. Kosowsky, and A. Stebbins, Phys. Rev. Lett. **78**, 2058 (1997); Phys. Rev. D **55**, 7368 (1997).
 - [12] P. Bender *et al.*, "LISA Pre-Phase A Report" (second edition) (1998).
 - [13] N. Seto, S. Kawamura, and T. Nakamura, Phys. Rev. Lett. **87**, 221103 (2001); S. Kawamura *et al.*, Class. Quant. Grav. **23**, S125 (2006).
 - [14] S. Phinney *et al.*, NASA Mission Concept Study, [http://universe.nasa.gov/program/bbo.html]; G. M. Harry, P. Fritschel, D. A. Shaddock, W. Folkner and E. S. Phinney, Class. Quant. Grav. **23**, 4887 (2006) [Erratum-ibid. **23**, 7361 (2006)].
 - [15] E. Gustafson, D. Shoemaker, K. A. Strain, and R. Weiss, LIGO Document No. T990080-00-D (www.ligo.caltech.edu/docs/T/T990080-00.pdf); P. Fritschel, Proc. SPIE, **4856**, 282 (2003).
 - [16] K. Kuroda *et al.*, Class. Quantum Grav. **23** S215.
 - [17] A. Nishizawa *et al.*, Phys. Rev. D **77**, 022002 (2008); A. Nishizawa *et al.*, arXiv:0801.4149 [gr-qc]; T. Akutsu *et al.*, arXiv:0803.4094 [gr-qc].
 - [18] D. Baumann, P. Steinhardt, K. Takahashi and K. Ichiki, Phys. Rev. D **76**, 084019 (2007).
 - [19] C. Carbone, C. Baccigalupi and S. Matarrese, Phys. Rev. D **73**, 063503 (2006).
 - [20] D. J. Schwarz, Mod. Phys. Lett. A **13**, 2771 (1998).
 - [21] S. Weinberg, Phys. Rev. D **69**, 023503 (2004).
 - [22] Y. Watanabe and E. Komatsu, Phys. Rev. D **73**, 123515 (2006).
 - [23] L. A. Boyle and P. J. Steinhardt, astro-ph/0512014.
 - [24] M. S. Turner, Phys. Rev. D **55**, R435 (1997).
 - [25] T. L. Smith, M. Kamionkowski and A. Cooray, Phys. Rev. D **73**, 023504 (2006); arXiv:0802.1530 [astro-ph].
 - [26] B. C. Friedman, A. Cooray and A. Melchiorri, Phys. Rev. D **74**, 123509 (2006).
 - [27] J. R. Pritchard and M. Kamionkowski, Annals Phys. **318**, 2 (2005).
 - [28] M. Maggiore, Phys. Rep. 331 (2000) 283-367.
 - [29] J. E. Lidsey *et al.*, Rev. Mod. Phys. **69**, 373 (1997).
 - [30] A. Kosowsky and M. S. Turner, Phys. Rev. D **52**, R1739 (1995).
 - [31] A. D. Dolgov and A. D. Linde, Phys. Lett. B **116**, 329 (1982).
 - [32] L. F. Abbott, E. Farhi and M. B. Wise, Phys. Lett. B **117**, 29 (1982).
 - [33] E. W. Kolb and M. S. Turner, *The Early Universe* (Westview Press, Boulder, CO, 1990).
 - [34] L. Kofman, A. Linde and A. A. Starobinsky, Phys. Rev. D **56**, 3258 (1997).
 - [35] J. H. Traschen and R. H. Brandenberger, Phys. Rev. D

- 42**, 2491 (1990).
- [36] L. Kofman, A. Linde and A. A. Starobinsky, Phys. Rev. Lett. **76**, 1011 (1996).
 - [37] R. Easther, J. T. Giblin and E. A. Lim, Phys. Rev. Lett. **99**, 221301 (2007).
 - [38] J. Garcia-Bellido and D. G. Figueroa, Phys. Rev. Lett. **98**, 061302 (2007); J. Garcia-Bellido, D. G. Figueroa and A. Sastre, Phys. Rev. D **77**, 043517 (2008).
 - [39] J. F. Dufaux, A. Bergman, G. Felder, L. Kofman, and J. P. Uzan, Phys. Rev. D **76**, 123517 (2007).
 - [40] D. N. Spergel *et al.*, Astrophys. J. Suppl. **170**, 377 (2007).
 - [41] T. Chiba, Y. Himemoto, M. Yamaguchi and J. Yokoyama, Phys. Rev. D **76**, 043516 (2007).
 - [42] U. Seljak *et al.*, Phys. Rev. D **71**, 103515 (2005).
 - [43] M. Kamionkowski, A. Kosowsky, and M.S. Turner, Phys. Rev. D **49**, 2837 (1994).
 - [44] M. Kawasaki, K. Kohri and T. Moroi, Phys. Lett. B **625**, 7 (2005).
 - [45] K. Nakayama, S. Saito, Y. Suwa and J. Yokoyama, arXiv:0804.1827 [astro-ph].
 - [46] S. Kuroyanagi *et al.*, in preparation.
 - [47] M. Morikawa and M. Sasaki, Prog. Theor. Phys. **72**, 782 (1984).
 - [48] Y. Shtanov, J. Traschen and R. Brandenberger, Phys. Rev. D **51**, 5438 (1995).
 - [49] S. Coleman, and E. Weinberg, Phys. Rev. D **7**, 1888 (1973).
 - [50] A. Linde, Phys. Rev. D **49**, 748 (1994).
 - [51] J. Garcia-Bellido, and A. Linde, Phys. Rev. D **57**, 6075 (1998).
 - [52] H. Kudoh, A. Taruya, T. Hiramatsu and Y. Himemoto, Phys. Rev. D **73**, 064006 (2006).